



A Hybrid Reconfigurability Structure for a Novel 5G Monopole Antenna for Future Mobile Communications at 28/38 GHz

M. Kamran Shereen^{1,2} · M. I. Khattak¹

Received: 13 March 2020 / Accepted: 9 June 2021 / Published online: 20 June 2021
© King Fahd University of Petroleum & Minerals 2021

Abstract

This study proposes a novel reconfigurable antenna for the millimeter-wave frequency spectrum. The proposed hybrid reconfigurable antenna is designed to reconfigure antenna parameters in compliance with wireless application specifications, such as frequency and radiation patterns. PIN Diodes as a switch are used to monitor the reconfiguration features i.e. adjusting the frequency response and radiation pattern of the antenna. For the desired goal, antenna is incorporated with three switches (S_1 , S_2 & S_3). The main beam of the antenna is guided by S_1 and S_2 which connects parasitic stubs H_1 and H_2 and the frequency is controlled by S_3 between 28 and 38 GHz which connects patch P_1 with P_2 . Proposed work is validated for 28 GHz and 38 GHz operational bands. When S_3 is active (at ON state), the proposed antenna operates at 28 GHz resonant frequency with a reflection coefficient of -32.3 dB and when S_3 is in-active (at OFF state), it results in 38 GHz resonant frequency with a reflection coefficient of -42.1 dB. RTDuroid5880 with $\epsilon_r = 2.33$, $\tan \delta = 0.0009$ and thickness (h) of 0.506 mm and is excited through an inset feed. HFSS software is used for the simulation purpose.

Keywords Frequency and radiation pattern reconfigurable antenna · HYBRID reconfigurable 5G mobile communication · millimeter waves · microstrip patch antenna

1 Introduction

It is expected that by the end of 2021, the next generation of telecommunications networks (fifth generation or 5G) will hit the market and will continue to expand globally. 5G is expected to create a large IoT (Internet of Things) ecosystem in addition to data rate enhancement, in which networks can meet the connectivity needs and demands of billions of linked devices, coping with speed, latency and costs as necessary. For 5G networks (millimeter waves between 30 and 300 GHz), using lower frequencies is why 5G can be faster. By transmitting information through millimeter waves [1], 5G mobile communications systems have a major effect on modern technology. As an example of progressive improvements in the network interface [2], compared with current cellular

infrastructure, this represents a major move forward. 28 GHz and 38 GHz [3] are the major bands intended for the future 5G mobile wireless networks and to fulfill bandwidth requirements. As regards the analysis of the under-used mm-wave frequency range, several works on the propagation study of cellular mm-wave in densely populated environments [4–8] using various shapes of smart antennas have been published for future broadband wireless communication networks. For instance, T. Recently, Rappaport et al. published detailed propagation observation campaigns at 28 GHz and 38 GHz bands to provide insight into their indoor and environmental applicability in Austin and New York City [9]. In addition, narrowband and wideband observations have been carried out under various indoor and outdoor conditions to allow precise predictive models to be generated for 60 GHz radio channels [10]. But there are limitations in the antenna designs used in this literature in terms of cost, size and complex circuitry. Use of the reconfigurable antennas, on the other hand, is another interesting and exciting approach to the new developments in wireless communications networks [11]. This community of antennas helps to reconfigure not only the bandwidth, but also the radiation and polarization

✉ M. Kamran Shereen
enrkamran@uetpeshawar.edu.pk

¹ Electrical Engineering Department, University of Engineering and Technology, Peshawar 25120, Pakistan

² United States Pakistan Centre for Advanced Studies in Energy (USPCASE), UETP, Peshawar, Pakistan



patterns. Once it provides agile frequency, the reconfigurable antenna offers flexibility in architecture, using specified operating system and cognitive radios to deal with multi-service, multi-standard and multi-band operations that can be extended and reconfigured. Furthermore, using reconfiguration, an efficient utilization range as well as power consumption is achieved. The Adaptive and Cognitive Radio over Fiber (ACROF) concept [12] is recently proposed, focusing on the combination of optically controlled reconfigurable antennas and ROF systems [13]. A high-capacity optical back-haul with a wireless, energy and spectrum-efficient remote access module is feasible using this new approach, and fresh optical advantages are also being used. A lightweight, reconfigurable hybrid antenna is presented by the authors of [14], which has two connectors used for switching the surface current distribution, frequency and radiation pattern of the antenna. In the different wireless communication bands with steerable beam pattern designed on graphene pads, the reconfigurable 5G to 4G operating band for radio frequency energy harvesting (RF-EH) is suggested [15]. A reconfigurable microstrip ultra-wide band (UWB) antenna, where frequency and pattern switching operating within the 3 GHz to 10 GHz frequency range is presented by the authors of [16]. Using PIN diodes or NMOS transistor as switching instruments, reconfigurability of the frequency and pattern is achieved [16]. A basic pattern reconfigurable printed Inverted-F antenna composed of one main radiator and one parasitic component is proposed for WLAN applications with low profile monopole antenna [17]. The proposed antenna, using only one PIN diode, can change the pattern and the polarization over the entire 205 MHz range.

This research work provides a state-of-the-art method for introducing hybrid reconfigurable features of frequency and radiation pattern in a microstrip patch antenna. Depending on the state of the lumped switch S_3 , the proposed antenna operates at the desired frequency bands of 28 GHz and 38 GHz, while the other two switches, S_1 and S_2 are installed in the ground to create reconfigurability of the radiation pattern.

2 Statistics of Reconfigurable Antenna Patch

The proposed reconfigurable patch antenna model typically consists of a patch, often manufactured on a substrate and ground with Lumped parameter. Five geometric parameters (L, W, g, L_d and LP_k) (Eq. 1.) adjusted for k th number of lumped parameter [18, 19] are included in the architecture of the HRA with inset feed and consist of three layers including patch substrate and parasitic stubs.

Whereas both the parasitic stubs and the patch of the antenna can be connected via LP_k (k th number of Lumped Parameter, used for switching purpose).

$$\begin{cases} \Phi(W, L, y_0, g, W_0, LP_k) = [\delta B, \delta A_e, \delta G]. W^T \\ Obj.Fun = \min \Phi(W, L, y_0, g, LP_k) \end{cases} \quad (1)$$

W , width of patch; L , length of patch; y_0 , any required slot length; g , notch width; W_0 , feed width of patch

$$W = \frac{c}{2f_0 \sqrt{\frac{\epsilon_{eff} + 1}{2}}} \quad (2)$$

ϵ_{eff} , effective dielectric constant; f_0 , resonant frequency.

Because of the fringing fields and effective dielectric constant Eq. (3), length of the patch is calculated from Eq. (5);

$$\epsilon_{eff} = \frac{\epsilon_r + 1}{2} + \frac{\epsilon_r - 1}{2} \left(\frac{1}{\sqrt{1 + 12 \left(\frac{h}{W} \right)}} \right) \quad (3)$$

ϵ_r , dielectric constant of material; h , separation of the trace from the ground (thickness).

Patch Length:

$$L = L_{eff} - 2\Delta L \quad (4)$$

Effective Length:

$$L_{eff} = \frac{c}{2f_0 \sqrt{\epsilon_{eff}}} \quad (5)$$

$$\Delta L = 0.412h \left[\frac{(\epsilon_{eff} + 0.3) \left(\frac{W}{h} + 0.264 \right)}{(\epsilon_{eff} - 0.258) \left(\frac{W}{h} + 0.8 \right)} \right] \quad (6)$$

where $\delta F, \delta B, \delta A_e$ and δR_L shows the deviation between the performance of the simulated reconfigurable antenna and the performance of the measured reconfigurable antenna (Fig. 1). LP_k (k th number of Lumped Parameters) is actually the forward biased (ON State) and Reversed biased (OFF State) characteristics of a switch (PIN Diode, D_k) in this case.

2.1 ON State (Forward Biased)

When a PIN diode is forward biased, holes and electrons are injected from the P and N regions into the I -region (as shown in Fig. 3a–c). These charges do not recombine immediately. Instead, a finite quantity of charge always remained stored and results in a lowering of the resistivity of the I -region (Eqs. 7–10).

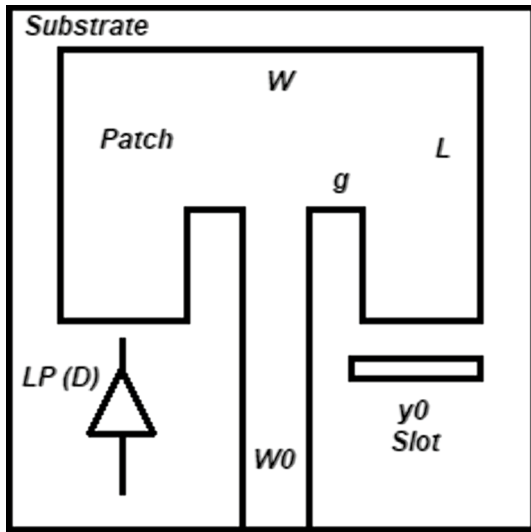


Fig. 1 General architecture of reconfigurable antenna

$$Q = I_F \tau \tag{7}$$

Quality of stored charge depends on τ , Recommendation or carrier life time; I_F Forward biased current.

The resistance of the I -region under forward bias, R_S is inversely proportional to Q and may be expressed as.

Where,

$$R_S = \frac{W_I^2}{(\mu_N + \mu_p)Q} \tag{8}$$

W_p , I -region width; μ_N , electron mobility; μ_p , hole mobility.

From Eqs. 2 and 3, R_S as inverse function of current is

$$R_S = \frac{W_I^2}{(\mu_N + \mu_p)\tau I_F} \tag{9}$$

Equation 4 is valid over an extremely high frequency range PIN diodes are used in a circuit.

Hence,

$$D_k(\text{ON state}) = R_{Sk} = \frac{W_{I(k)}^2}{(\mu_{N_k} + \mu_{P_k})\tau_k I_{F_k}} \tag{10}$$

where k is from $1 \leftrightarrow N$ th.

2.2 OFF State (Reversed Biased)

At high RF frequencies when a PIN diode is reverse biased, it appears as a parallel plate capacitor, essentially independent of reverse voltage, having a value of (Eqs. 11–13).

$$C_T = \frac{\epsilon A}{W} \tag{11}$$

ϵ , silicon dielectric constant; A , junction area; W , I -region thickness.

The lowest frequencies at which this effect begins to predominate is related to the dielectric relaxation frequency of the I -region, f_τ , which may be computed as

$$f_\tau = \frac{I}{2\pi\rho\epsilon} \tag{12}$$

where, ρ , I -region resistivity.

Hence,

$$D_k(\text{OFF state}) = C_{T_k} = \frac{\epsilon_k A_k}{W_k} \tag{13}$$

where k from $1 \leftrightarrow N$ th.

3 Proposed Reconfigurable Antenna Architecture

A 28/38 GHz reconfigurable antenna is proposed in this section (Fig. 2a) and is fabricated depicted in Fig. 2c, d. The tiny geometry of the antenna is $23 \text{ mm} \times 25 \text{ mm} \times 0.506 \text{ mm}$ is excited through a $\frac{1}{4}$ transformer with a width of $w_1 = 1.1 \text{ mm}$ to the 50Ω microstrip line with a width of $w_7 = 2.5 \text{ mm}$. The antenna dimensions are tabulated in Table 1.

To calculate the patch width (W), effective permittivity (ϵ_{eff}), patch length (L), effective length (L_{eff}), and additional patch length (ΔL) Eqs. (2) to (6) are used [18]. The following procedure was adopted for a simple patch of 38 GHz, which was further modified by introducing stubs and lumped parameters.

Using Eqs. 2–6, Calculation for 38 GHz Frequency.

From Eq. 2

$$W = \frac{3 \times 10^8}{2(38 \times 10^9) \sqrt{\frac{2.33+1}{2}}} \tag{14}$$

$$W = 3 \text{ mm}$$

By placing Eq. 14 in 3, we get

$$\epsilon_{\text{eff}} = \frac{2.33 + 1}{2} + \frac{2.33 - 1}{2} \left(\frac{1}{\sqrt{1 + 12 \left(\frac{0.506}{3} \right)}} \right) \tag{15}$$

$$\epsilon_{\text{eff}} = 2$$

Similarly,

Fig. 2 Proposed antenna structure **a** proposed antenna **b** fabricated front and back view of prototype in anechoic chamber **c** fabricated prototype front view **d** fabricated prototype back view

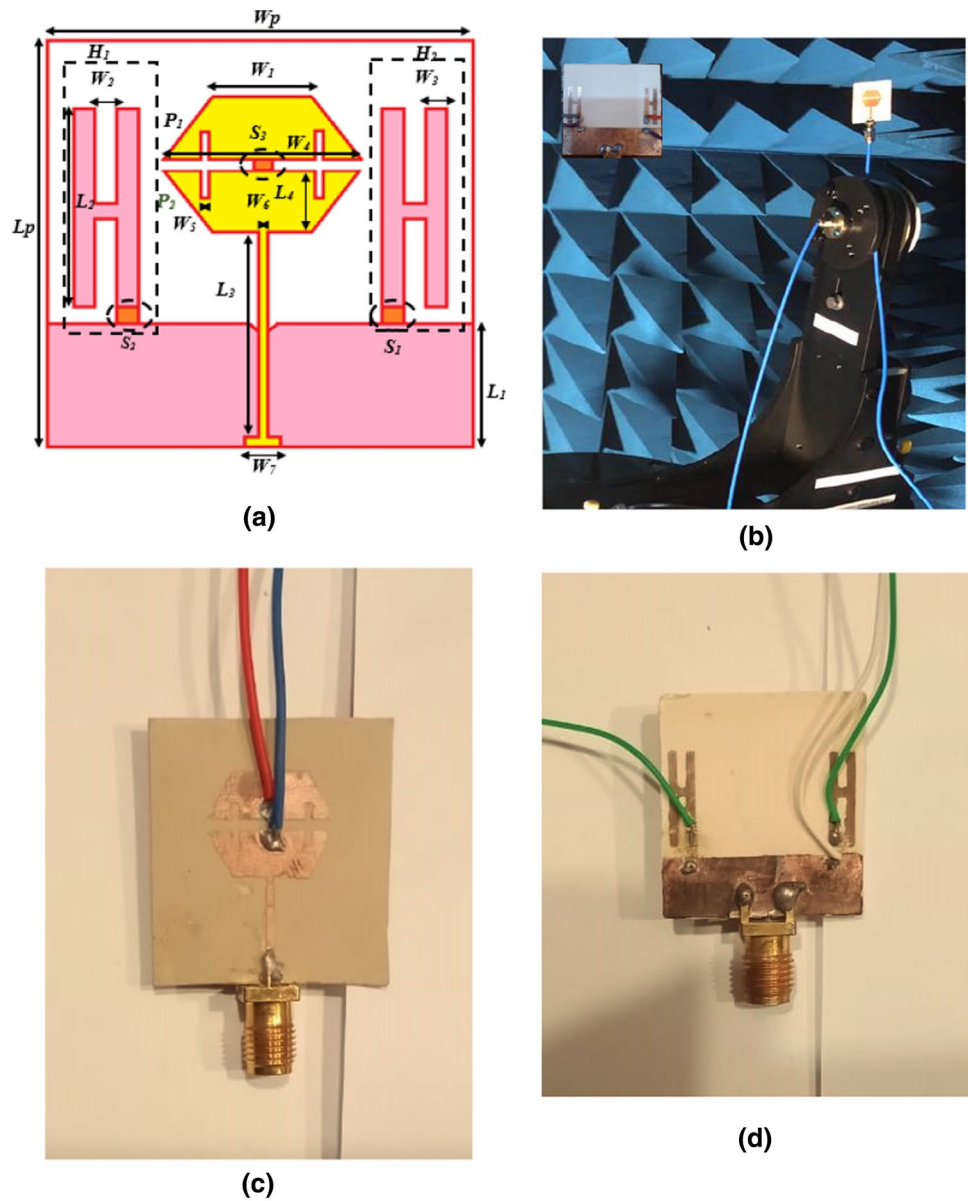


Table 1 Different parameter with their values of the proposed antenna

| Parameter | Dimensions (mm) | Parameter | Dimensions (mm) |
|-----------|-----------------|-----------|-----------------|
| W_p | 23 | L_p | 25 |
| W_1 | 6.5 | L_1 | 7 |
| W_2 | 2.2 | L_2 | 11.5 |
| W_3 | 2.2 | L_3 | 14.2 |
| W_4 | 8.4 | L_4 | 4.5 |
| W_5 | 1.1 | W_7 | 2.5 |
| W_6 | 1.1 | | |

$$L_{\text{eff}} = \frac{3 \times 10^8}{2(38 \times 10^9)\sqrt{2}}$$

$$L_{\text{eff}} = 2.8 \text{ mm} \tag{16}$$

From Eq. 6

$$\Delta L = 0.412(0.506) \left[\frac{(2 + 0.3) \left(\frac{3}{0.506} + 0.264 \right)}{(2 - 0.258) \left(\frac{3}{0.506} + 0.8 \right)} \right]$$

$$\Delta L = 0.4 \text{ mm} \tag{17}$$

Therefore, from Eqs. 16 and 17, we get

$$L = 2.8 - 2(0.4)$$

$$L = 2 \text{ mm} \tag{18}$$

Similar procedure was also adopted for 28 GHz frequency. ON/OFF states are operated by using the PIN diode as a switch. An inductor in series with a resistor is used for the ON state, while in parallel with a capacitor for the OFF state, with reference to the compatibility list of PIN diode SPDT switch (Fig. 3).

4 Results and Discussion

The reflection coefficients for different combinations of bias voltages covering the configured frequency band are shown in this section. Return loss (RL) of the proposed antenna is reconfigured under ON and OFF states of S_3 . The proposed architecture was selected according to the standard requirements of 5G cellular communication. The circuit board was fabricated using a procedure of optic-radiation of photolithography, which processed the photoresist layer to paste the mask onto silicon sheets. The proposed antenna was designed in a high frequency structure simulator Electromagnetics Suit, Ansys, Canonsburg, PA, USA, HFSS (High Frequency Structure Simulator) 19.2 3D electromagnetic field for the radio frequency and wireless design, and was measured using a ZVA 40 GHz vector network analyzer.

The reflection coefficients for different combinations of bias voltages covering the tuning frequency band are shown. The return loss S_{11} (dB) response of the proposed antenna has been made reconfigurable under ON and OFF states of the Switch 3 and can be viewed in Fig. 4a, b. Switch 3 can be seen clearly, which causes the frequency reconfiguration, between 28 and 38 GHz. Effects of various states of switches as given in Table 2, are discussed. During Case1 (from Model-Mode3) S_3 is kept ON (connecting P_1 & P_2), for 28 GHz which results in an RL of app. -32.3 dB as shown in Fig. 4a. Similarly, when P_1 & P_2 are disconnected (Case2) by deactivation of S_3 (OFF position), results in a RL of app. -42.1 dB at resonant frequency of 38 GHz, as shown in Fig. 4b. At both the cases, different modes of switches are summarized in Table 2.

Figure 4c, d shows the simulated and measured VSWR for every case (from Table 2). The results show that, the impedance bands were 1.51 GHz and 1.57 GHz for 28 GHz and 38 GHz (<2.5 standards, respectively).

The size and configuration of the ground plane is an important factor in the assessment of the impedance and radiation properties of the antenna due to time variations on the ground plane. The addition of H-shaped stub on the surface has very little effect on impedance, but there is a huge impact on the proposed antenna radiations. In all switching

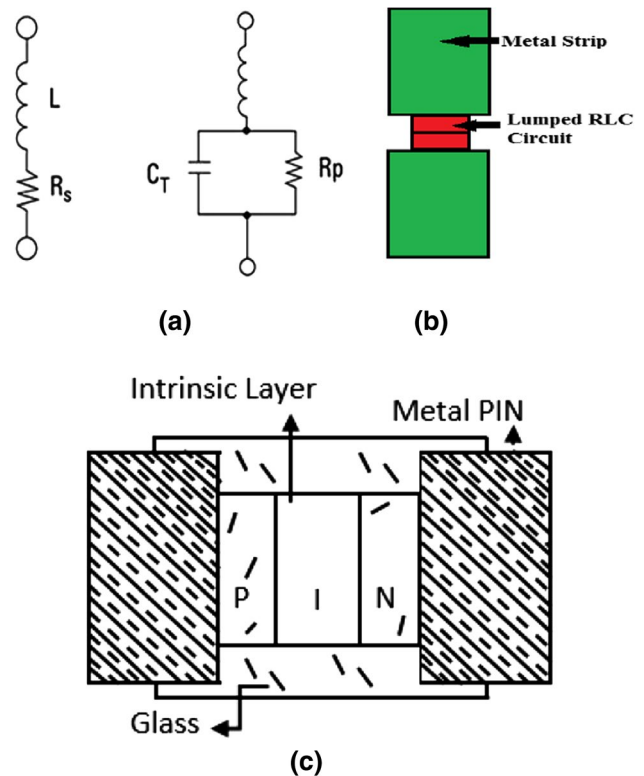


Fig. 3 PIN diode equivalent circuit a forward bias and revers bias ON/OFF states b equivalent simulator model c cross section basic PIN diode

conditions, there is a particular current distribution that contributes to the specific beam steering trend.

Figure 5 shows radiation pattern results from Table 3 (Mode 1 to 6). It illustrates that at Case 1, when S_3 is ON, the antenna operates with a resonant frequency of 28 GHz (it is unconcerned with 38 GHz). At this stage, the radiation beam direction of the antenna is such as, it radiates between 90° to 270° at Mode 1 (S_1 and S_2 both are at ON position) (Fig. 5a), 0° to 180° at Mode 2 (S_1 is at ON position and S_2 is at OFF position) (Fig. 5b), and 180° to 360° at Mode 3 (S_1 is at OFF position and S_2 is at ON position) (Fig. 5c). Similarly, during Case 2, when S_3 is kept OFF and proposed antenna resonates at 38 GHz, the beam direction is rotated as, it radiates between 90° to 270° at Mode 4 (S_1 and S_2 both are at ON position) (Fig. 5d), 0° to 180° at Mode 5 (S_1 is at ON position and S_2 is at OFF position) (Fig. 5e), and 180° to 360° at Mode 6 (S_1 is at OFF position and S_2 is at ON position) (Fig. 5f).

The changing positions of the pattern (anti-clockwise) cause the surface current density to vary, due to the connecting parasitic stubs H. Depending on the number of stubs, we can increase/decrease the steering angle (45° shift is used in this paper). Gain and efficiency with optimal values have been shown in Table 3. The acceptable level of VSWR for

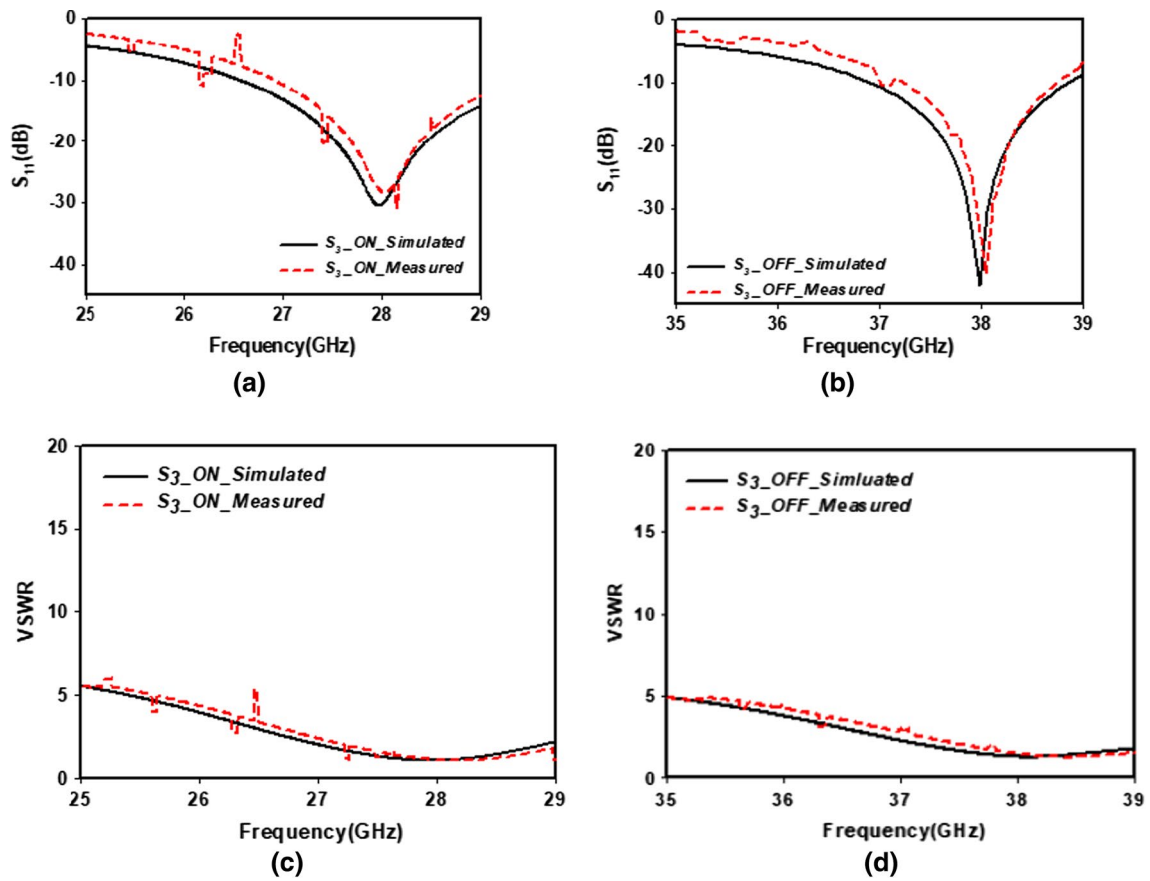


Fig. 4 Reflection coefficient at a S_3 is OFF b S_3 is ON c VSWR at S_3 ON and d VSWR at S_3 OFF

Table 2 Different cases of switches

| Cases | Modes | S_1 | S_2 | S_3 | Frequency (GHz) | Angle of radiation pattern |
|-------|-------|-------|-------|-------|-----------------|-------------------------------------|
| Case1 | Mode1 | ON | ON | ON | 28 | between 90° and 270° |
| | Mode2 | ON | OFF | ON | 28 | between 0° and 180° |
| | Mode3 | OFF | ON | ON | 28 | between 180° and 360° |
| Case2 | Mode4 | ON | ON | OFF | 38 | between 90° and 270° |
| | Mode5 | ON | OFF | OFF | 38 | between 0° and 180° |
| | Mode6 | OFF | ON | OFF | 38 | between 180° and 360° |

Fig. 5 Radiation pattern at **a** Mode1 **b** Mode2 **c** Mode3 **d** Mode4 **e** Mode5 **f** Mode6

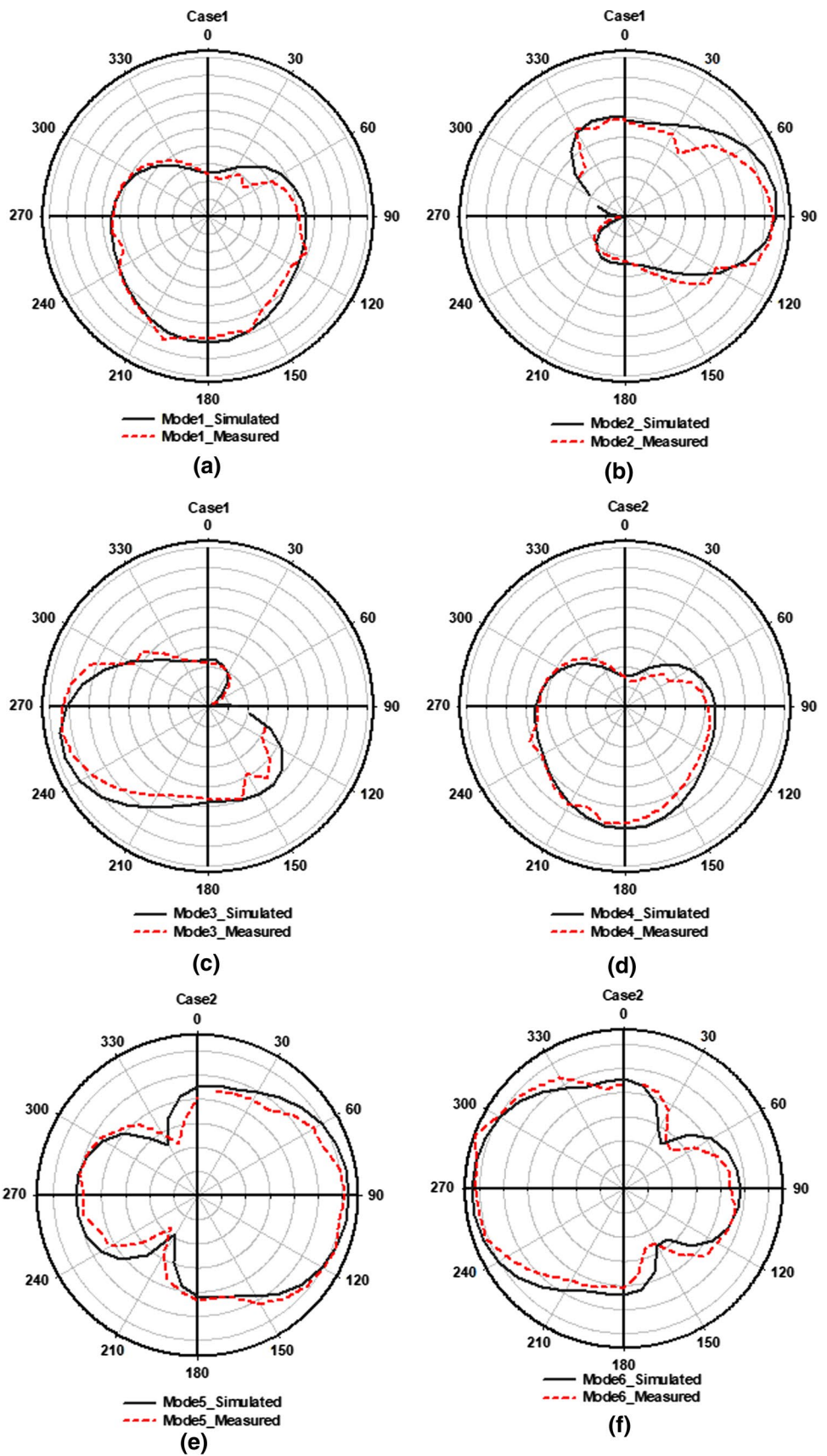


Table 3 Gain and efficiency for mode1 and mode4

| State | Gain (dBi) | Efficiency (%) |
|-------|------------|----------------|
| Mode1 | 9.2 | 95 |
| Mode4 | 10.3 | 93 |

Table 4 Performance comparison with previously published work

| References | Reconfiguration | Size (mm) | Band (GHz) | Actuators | Generation |
|-----------------------------|-----------------|-----------|-----------------|--------------|------------|
| Fang et al. [20] | Compound/hybrid | 41×47×1.6 | 2.1–2.4 | 4PIN diodes | 4G |
| Kimouche and Mansoul [21] | Compound/hybrid | 60×50×0.4 | 5.8 | 11PIN diodes | 4G |
| Abutarboush and Shamim [22] | Compound/hybrid | 50×50 | 4.3 | 3PIN diodes | 4G |
| Rao et al. [23] | Compound/hybrid | 43×28×0.2 | 2.3–3.8,4.5–5.1 | 6PIN diodes | 4G |
| This work 38 GHz | Compound/hybrid | 23×25 | 36.3–39.7 | 3PIN diodes | 5G |
| This work 28 GHz | Compound/hybrid | 23.5×25.5 | 27.1–29.8 | 3PIN diodes | 5G |

wireless application should be less than 2 dB as shown in Fig. 4c, d.

5 Conclusion

A novel lightweight hybrid reconfigurable antenna is modeled and experimentally tested in this research work for pattern and frequency switching between 28 and 38 GHz resonant frequencies. RTDuroid5880 with $\epsilon_r = 2.33$, $\tan \delta = 0.0009$ and thickness (h) of 0.506 mm is used as a substrate material and the antenna is excited through an inset feed. The designed antenna can be utilized for advanced 5G mobile communication applications due to its competitive features. Depending on the states of S_1 , S_2 & S_3 frequency and radiation pattern switching is achieved. Main beam of the antenna is circulated through S_1 and S_2 by connecting parasitic stubs H_1 and H_2 and the frequency is configured by S_3 between 28 and 38 GHz (connecting patch P_1 with P_2). The proposed antenna operates at 28 GHz @RL ≤ -32.3 dB and when S_3 is in-active (at OFF state), it results in RL ≤ -42.1 dB at 38 GHz (published literature comparison is presented in Table 4).

Declarations

Conflict of interest The authors declare no conflict of interest.

References

- Ericsson Technology Review, Designing for the future: the 5G NR physical layer. <https://www.ericsson.com/en/ericsson-technology-review/archive/2017/designing-for-the-future-the-5g-nr-physical-layer>
- Hu, G.H.; Feng, J.; Zhang, S.; Cung, G.; Bernhard, J.T.: Directional reconfigurable antennas on laptop computers: simulation, measurement and evaluation of candidate integration positions. *IEEE Trans. Antennas Propag.* **52**(12), 3220–3227 (2004)
- Stöhr, A., et al.: Millimeter-wave photonic components for broadband wireless systems. *IEEE Trans. Microw. Theory Tech.* **58**(11), 3071–3082 (2010). <https://doi.org/10.1109/TMTT.2010.2077470>
- Iqbal, N., et al.: Frequency and bandwidth dependence of millimeter wave ultra-wide-band channels. In: 2017 11th European Conference on Antennas and Propagation (EUCAP), Paris, pp. 141–145. (2017). <https://doi.org/10.23919/EuCAP.2017.7928850>
- Rahman, S.; Robertson, D.: Time-frequency analysis of millimeter-wave radar micro-Doppler data from small UAVs. In: 2017 Sensor Signal Processing for Defence Conference (SSPD), London, pp. 1–5. (2017). <https://doi.org/10.1109/SSPD.2017.8233269>
- Rappaport, T.S., et al.: Millimeter wave mobile communications for 5G cellular: it will work! *IEEE Access* **1**, 335–349 (2013). <https://doi.org/10.1109/ACCESS.2013.2260813>
- Ismail, M.F.; Rahim, M.K.A.; Majid, H.A.: The investigation of PIN diode switch on reconfigurable antenna. In: 2011 IEEE International RF & Micro-wave Conference, Seremban, Negeri Sembilan. (2011). pp. 234–237.
- Wang, L.; Yu, J.; Li, Y.: Microwave photonic antenna for fiber radio application. In: 2018 IEEE 3rd Optoelectronics Global Conference (OGC), Shenzhen, pp. 122–125. (2018). <https://doi.org/10.1109/OGC.2018.8529927>
- Kim, J., et al.: MIMO-supporting radio-over-fiber system and its application in mmWave-based indoor 5G mobile network. *J. Lightw. Technol.* **38**(1), 101–111 (2020). <https://doi.org/10.1109/JLT.2019.2931318>
- Douville, R.; Roscoe, D.; Cuhaci, M.; Stubbs, M.: Antennas for broadband microwave/mm-wave communication systems. In: Luise, M.; Pupolin, S. (Eds.) *Broadband Wireless Communications*. Springer, London (1998). https://doi.org/10.1007/978-1-4471-1570-0_14
- Alipour, S.; Parvaresh, F.; Ghajari, H.; Donald, F.K.: Propagation characteristics for a 60 GHz wireless body area network (WBAN). In: 2010—MILCOM 2010 Military Communications Conference, San Jose, CA, pp. 719–723. (2010). <https://doi.org/10.1109/MILCOM.2010.5680295>
- Guo, Y.J.; Qin, P.Y.: Reconfigurable antennas for wireless communications. In: Chen, Z.; Liu, D.; Nakano, H.; Qing, X.;



- Zwick, T. (Eds.) Handbook of Antenna Technologies. Springer, Singapore (2016). https://doi.org/10.1007/978-981-4560-44-3_119
13. Qin, P.Y.; Guo, Y.J.; Liang, C.H.: Effect of antenna polarization diversity on MIMO system capacity. *IEEE Antennas Wirel. Propag. Lett.* **9**, 1092–1095 (2010)
 14. Kamran Shereen, M.; Khattak, M.I.; Witjaksono, G.: A brief review of frequency, radiation pattern, polarization, and compound reconfigurable antennas for 5G applications. *J. Comput. Electron.* **18**, 1065–1102 (2019). <https://doi.org/10.1007/s10825-019-01336-0>
 15. Li, X.; Tsui, C.; Ki, W.: UHF energy harvesting system using reconfigurable rectifier for wireless sensor network. In: 2015 IEEE International Symposium on Circuits and Systems (ISCAS), Lisbon. pp. 93–96. (2015). <https://doi.org/10.1109/ISCAS.2015.7168578>
 16. Shereen, M.K.; Khattak, M.I.; Al-Hasan, M.: A frequency and radiation pattern combo-reconfigurable novel antenna for 5G applications and beyond. *Electronics* **9**, 1372 (2020)
 17. Elsheakh, D.N.: Frequency reconfigurable and radiation pattern steering of monopole antenna based on graphene pads. In: 2019 IEEE-APS Topical Conference on Antennas and Propagation in Wireless Communications (APWC), Granada, Spain. pp. 436–440 (2019).
 18. Shereen, M.K.; Khattak, M.I.; Al-Hasan, M.: A hybrid reconfigurability structure for a novel 5G monopole antenna for future mobile communication. *Frequenz* (2020). <https://doi.org/10.1515/freq-2020-0031>
 19. Skaik, T.; AbuJalambo, M.: Design of microstrip circular UWB antenna with reconfigurable frequency and radiation pattern. In: 2018 International Conference on Promising Electronic Technologies (ICPET), Deir El-Balah. pp. 52–57 (2018)
 20. Fang, P.; Wang, K.; Wolfmüller, M.; Eibert, T.F.: Radiation pattern reconfigurable antenna for MIMO systems with antenna tuning switches. In: 2018 IEEE International Symposium on Antennas and Propagation & USNC/URSI National Radio Science Meeting, Boston, MA. pp. 503–504 (2018)
 21. Kimouche, H.; Mansoul, A.: A compact reconfigurable single/dual band antenna for wireless communications. In: Proceedings of the 5th European Conference on Antennas and Propagation, pp. 393–396 (2011).
 22. Abutarboush, H.F.; Shamim, A.: A reconfigurable inkjet-printed antenna on paper substrate for wireless applications. *IEEE Antennas Wirel. Propag. Lett.* **17**(9), 1648–1651 (2018)
 23. Rao, Q.; Denidni, T.A.; Sebak, A.R.; Johnston, R.H.: Compact independent dual-band hybrid resonator antenna with multifunctional beams. *IEEE Antennas Wirel. Propag. Lett.* **5**(1), 239–242 (2006)

